Azo-based phenylthiophene Schiff bases: Syntheses, crystal structures and optical properties

Afef Shili, Awatef Ayadi, Said Taboukhat, Nabil Zouari, Bouchta Sahraoui, Abdelkrim El-Ghayoury

Azo-based phenylthiophene Schiff bases: Syntheses, Crystal Structures and Optical Properties

Afef Shili[a], Awatef Ayadi[a,b], Said Taboukhat[b], Nabil Zouari[a]. Bouchta Sahraoui[b], Abdelkrim El-Ghayoury[b*]

[a]*Laboratoire de Physico-chimie de l'état solide, Département de Chimie, Faculté des sciences de Sfax, BP : 1171, 3000 Sfax, Université de Sfax, Tunisia.*

[b]*MOLTECH-Anjou, UMR 6200, CNRS, UNIV Angers, 2 bd Lavoisier, 49045 Angers, France.*

Corresponding authors:

Abdelkrim El-Ghayoury, e-mail: abdelkrim.elghayoury@univ-angers.fr

Abstract

Two new organic materials based donor acceptor systems, namely N,N-dimethyl-4-((E)-(4-((E)-((5-phenylthiophen-2-yl)methylene)amino)phenyl)diazenyl)aniline **A** and (E)-4-((E)-(4-nitrophenyl)diazenyl)-N-((5-phenylthiophen-2-yl)methylene)aniline **B** were successfully synthesized. Both compounds (**A** and **B**) have been synthesized by a condensation reaction between N, N-Dimethyl-4,4'-azodianiline or 4-(4-nitrophenylazo)aniline and 5-phenylthiophene-2-carbaldehyde, with 77% and 83% yield. These two compounds were subjected to the following characterization techniques: single crystal X-ray diffraction, elemental analysis, infrared, mass, ^{1}H NMR, ^{13}C NMR spectroscopy and thermogravimetric analysis. The Schiff bases **A** and **B** belong to the monoclinic $P2_1/c$ space group. Their crystal structures are stabilized by intra and intermolecular hydrogen bonds, as well as by weak π–π stacking. The prevalence of this interaction is illustrated by an analysis of the three dimensional Hirshfeld surface and by two-dimensional fingerprint plots. Optical properties of these compounds have been determined by UV-absorption spectroscopy, which disclosed the energy of the optical band gap.

Keywords: Azobenzene; Schiff base; Hydrogen bonds; UV-Vis absorption; Hirshfeld surface.

1. Introduction

Organic molecules which have in their structures an electron donor or acceptor units are among the most important conjugated organic materials and have attracted much attention because of their use as functional materials with low gap energy [1] and of their interesting structures [2]. In this type of compounds, electron donor and acceptor groups are connected via a conjugated π link. Adjustment of the different donor or acceptor entities in a donor-acceptor molecule (D-A) would alter its physical and chemical properties. Hence, organic materials appear as promising candidates for the production of transistors, photodiodes and biochemical sensors [3-5]. Azobenzene and its numerous derivatives is one of the greatest examined classes of organic compounds having interesting optical properties, which are necessary for their potential applications [6-8]. They have been attracted increasing attention since they can serve as electroactive and photoactive materials for many important applications such as optical storage media [9-11], nonlinear optics [12], chemosensors [13], optical switches [14] and solar cells [15]. As a result, large theoretical and experimental work has been distorted to research and study the structural and photochemical properties of azobenzene-based structures. Our interests have been in the synthesis, the characterization and the optical properties of azo-based phenylthiophene Schiff bases. Lately, thiophene nucleus presents a very important field in drug discovery because of their biological activities [16], more recently it was utilized in the growth of antibacterial agent [17,18]. Besides, thiophene plays a significant role as synthetic intermediates, for instance, in the production of new conductive polymers [19,20] or materials with nonlinear optical properties [20]. The combination between azobenzene and thiophene should lead to π-conjugated dyads exhibiting many interesting properties. Therefore, the present study deals with the synthesis, X-ray structures and the optical properties (including optical band gap determination) of two novel azo-phenylthiophene Schiff bases **A** and **B**.

2. Experimental section

Materials

All manipulations were performed in air using commercial grade solvents. N,N-Dimethyl-4,4'-azodianiline $C_{14}H_{16}N_4$ (97%), 4-(4-nitrophenylazo)aniline $C_{12}H_{10}N_4O_2$ (90%), 5-phenylthiophene-2-carbaldehyde $C_{11}H_8OS$ (98%) were procured from Sigma-Aldrich and employed without further purification.

Instrumentation

NMR spectra were recorded on a Bruker Avance DRX 300 spectrometer operating at 300 MHz for ^1H and 75 MHz for ^{13}C. Chemical shifts are expressed in parts per million (ppm) downfield from

external TMS. The following abbreviations are used: s, singlet; d, doublet; t, triplet; td, triplet of doublet. Infrared measurements employing (KBr pellets) was registered using a Perkin–Elmer FT-IR 1000 spectrometer. UV−visible spectra were recorded at room temperature in quartz cuvettes using Perkin-Elmer spectrophotometer. Elemental analyses (C, H and N) were performed on a Thermo-Scientific Flash 2000 Organic. Mass spectra were collected with Bruker Biflex-III TM. Thermogravimetric analysis (TGA) of the compounds was carried out using a Setaram 92 Thermal Analyser from room temperature up to 500°C with a heating rate of 10°C/min under an Oxygen atmosphere. X-ray single-crystal diffraction data for both compounds were collected on an Agilent SuperNova diffractometer equipped with Atlas CCD detector and mirror monochromated micro-focus Cu-Kα radiation (λ = 1.54184 Å). The crystal structures of **A** and **B** were solved in the monoclinic system, space group $P2_1/c$, according to the automated search for space group accessible in WingX [21] and to the systematic extinctions conditions. The two structures were solved by direct methods, expanded and refined on F^2 by full matrix least-squares techniques using SHELX programs (include SHELXS-97 and SHELXL-97, G.M. Sheldrick, 1998) [22]. All non-H atoms were refined anisotropically and the H atoms were included in the calculation without refinement. Multi-scan empirical absorption was corrected using the CrysAlisPro program (CrysAlisPro, Agilent Technologies, V1.171.37.35g, 2014). The graphical representation is provided with Diamond 2 [23] program. Details about data collection and solution refinement are given in **Table 1**. Crystallographic data for the structural analysis have been deposited with the Cambridge Crystallographic Data Center, CCDC 1900208 for **A** and CCDC 1900209 for **B**.

Synthesis of Schiff bases A and B

A solution of (E)-4-((4-aminophenyl)diazenyl)-N,N-dimethylaniline (0.200 g, 0.83 mmol) and 5-phenylthiophene-2-carbaldehyde (0.156 g, 0.83 mmol) in ethanol (30 mL) and a few drops of acetic acid were heated under reflux overnight. After cooling to room temperature, the precipitate formed was filtered off and washed with ethanol. The desired product **A** was obtained as red powder with a 77% yield. m.p: 247 °C.^{1}H NMR (300 MHz, $CDCl_3$) δ/ppm: 8.65(s, 1H, N=CH), 7.93 (dd, 4H, J = 4.4 Hz, J= 3.4 Hz, ArH),7.73 (d, 2H, J = 7.2 Hz, ArH), 7.52 (d, 1H, J = 3.7 Hz, ArH), 7.45 (d, 2H, J = 7.6 Hz, ArH), 7.39 (m, 4H, ArH), 6.81 (d, 2H, J = 9.0 Hz, ArH); 3.13 (s, 6H, 2(CH_3)).^{13}C NMR (75 MHz, $CDCl_3$) δ/ppm: 152.8(1C, N=CH), 152.3(ArC), 152.1(ArC), 151.4(ArC), 149.4(ArC), 143.9(ArC), 141.8(ArC), 133.8(ArC), 133.5(ArC), 129.1(ArC), 128.6(ArC), 126.1(ArC), 124.9(ArC), 123.8(ArC), 123.3(ArC), 121.8(ArC), 111.6(ArC), 40.3(2C, 2(CH_3)). Anal. Calc. for $C_{25}H_{22}N_4S$: C, 73.14 %; H, 5.40 %; N, 13.65 %. Found: C, 73.02 %; H, 5.33 %; N, 13.48 %.MALDI-

TOF MS calcd: m/z = 410.53 Da. Found: m/z = 410.50 HR-MS (M): for $C_{25}H_{22}N_4S$: 410.1556. Found: 410.59.

Compound **B** was obtained in the same way by using (E)-4-((4-nitrophenyl)diazenyl)aniline (0.200 g, 0.82 mmol) that was reacted with 5-phenylthiophene-2-carbaldehyde (0.154 g, 0.82 mmol) using ethanol as a solvent (20 mL) and a few drops of acetic acid. The desired product **B** was obtained as red powder with a 83% yield. m.p: 220 °C. ^{1}H NMR (300 MHz, $CDCl_3$) δ/ppm: 8.65 (s, 1H, N=CH), 8.43 (d, 2H, J= 8.9 Hz, ArH), 8.07 (d, 4H, J= 8.8 Hz, ArH), 7.75 (dd, 2H, J= 8.4 Hz, J= 6.8 Hz, ArH), 7.56 (d, 1H, J= 3.9 Hz, ArH), 7.48 (m, 2H, ArH), 7.42 (dd, 4H, J= 6.4 Hz, J= 2.2 Hz, ArH). ^{13}C NMR (75 MHz, CDCl3) δ/ppm: 155.9(ArC), 155.1(1C, N=CH), 153.9(ArC), 150.6(ArC), 150.3(ArC), 148.6(ArC), 141.4(ArC), 134.3(ArC), 133.6(ArC), 129.2(ArC), 128.8(ArC), 126.2(ArC), 124.9(ArC), 124.8(ArC), 123.9(ArC), 123.4(ArC), 122(ArC). Anal. Calc. for $C_{23}H_{16}N_4O_2S$: C, 66.97 %; H, 3.91 %; N, 13.58 %. Found: C, 66.78 %; H, 3.82 %; N, 13.49 %. MALDI-TOF MS calcd: m/z = 412.09 Da. Found: m/z = 413.4 HR-MS (M): for $C_{23}H_{16}N_4O_2S$: 412.0994. Found: 412.0997.

Hirshfeld surfaces and fingerprint plots

The inter contacts observed and two dimensional fingerprint plots of these two compounds **A** and **B** are measured graphically and visualized using Hirshfeld surface method. The Hirshfeld surfaces and the associated 2D fingerprint plots were calculated using Crystal Explorer [24]. We evaluate here the intermolecular interactions through inter contacts and then, we discuss the results.

3. Results and discussion

Synthesis and crystal structure description

Two types of azo-based phenylthiophene ligands which contain dimethylamino and nitro groups were synthesized. These two compounds **(A)** and **(B)** have been obtained by a condensation reaction between N,N-Dimethyl-4,4'-azodianiline or 4-(4-nitrophenylazo)aniline with 5-Phenylthiophene-2-carbaldehyde in ethanol. The protocol followed for the synthesis of the new systems is summarized in **Scheme 1**.

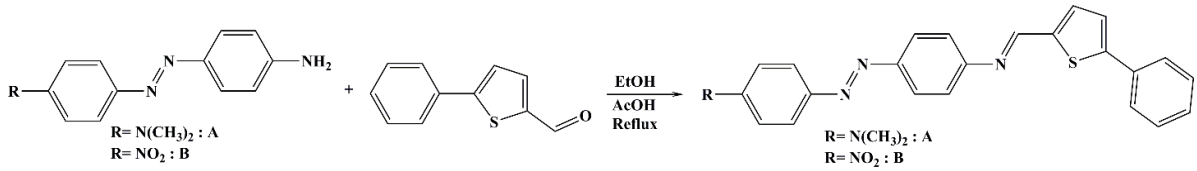

Scheme1: *Synthetic scheme of Schiff bases* ***A*** *and* ***B****.*

Both bases **A** and **B** crystallize in the monoclinic system space group P2 $_1$/c with one independent molecule in the unit cell. **(A)** and **(B)** differ only by the nature of the substitutions on the azobenzene

ring: **(A)** carries an electron donating dimethylamino group at the C21 para position while **(B)** is substituted by an electron acceptor nitro group at C21. The resutling crystal structures are depicted in **Figure1**. Both compounds **(A)** and **(B)** exhibit a regular spatial configuration with normal distances C–C single bonds, C=N imine bond (1.290(6) and 1.284(2) Å). In **A** and **B,** the distance C11–N1 being shorter than C12–N1 confirms the presence of the imine function.

As it can be seen in **Figure 1**, the two compounds are not completely planar. The distances between S1 and N1 in **(A)** and between S1 and N4 in **(B)** being of the order of 3.110 (3) and 3.106 (2) Å respectively, indicate the presence of an electronic delocalization in the two compounds The dihedral angles between the azobenzene unit and the 2-phenylthiophene group in both ligands are comparable: 35.38° for **(A)** and 35.78° for **(B)**. Selected parameters of the X-ray diffraction data collection and refinement are summarized in **Table**

1. Selected bond lengths and angles are depicted in **Table 2**.

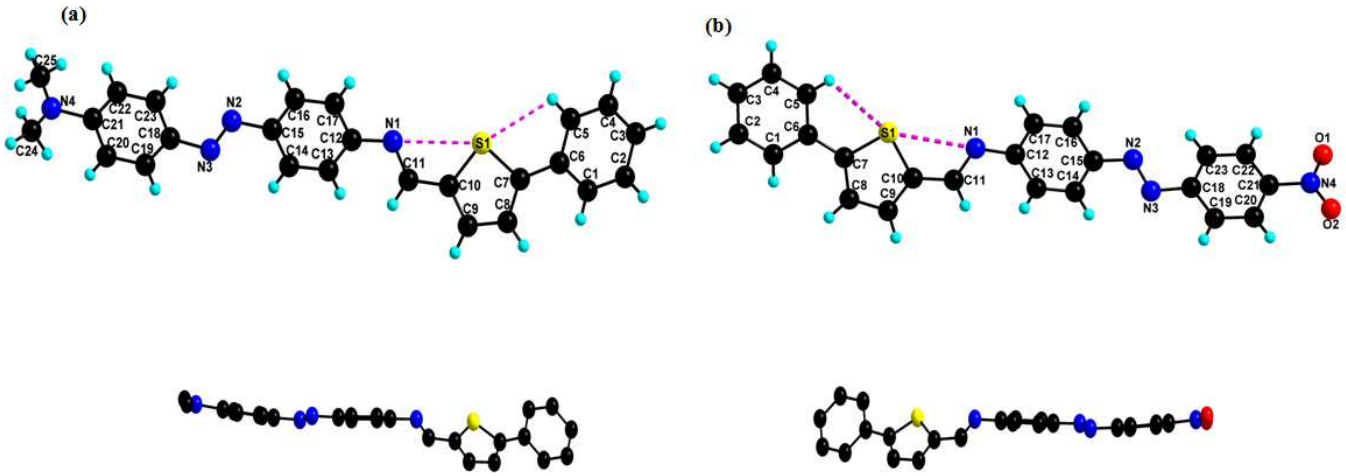

Figure 1*: Crystal structure of* ***A*** *(a) and* ***B*** *(b) with atom numbering scheme*

In the crystal structures formed by **A** and **B**, the sulfur atoms of thiophene moieties interact with the adjacent phenyl group via intramolecular C–H···S (C5–H5···S1 (2.79 Å), C5–H5···S1 (2.78 Å̊)) hydrogen bonds that make the thiophene unit and the phenyl ring coplanar. In the case of compound **B,** the presence of nitro group (-NO_2) has drastic consequences for the crystal packing. It leads indeed to the formation of intermolecular C–H···O hydrogen bond between Phenyl–C···H and NO_2 (Phenyl–C–H···O 2.687(7) Å) generating two-dimensional layers parallel to the (101) plan (**Figure 2**).

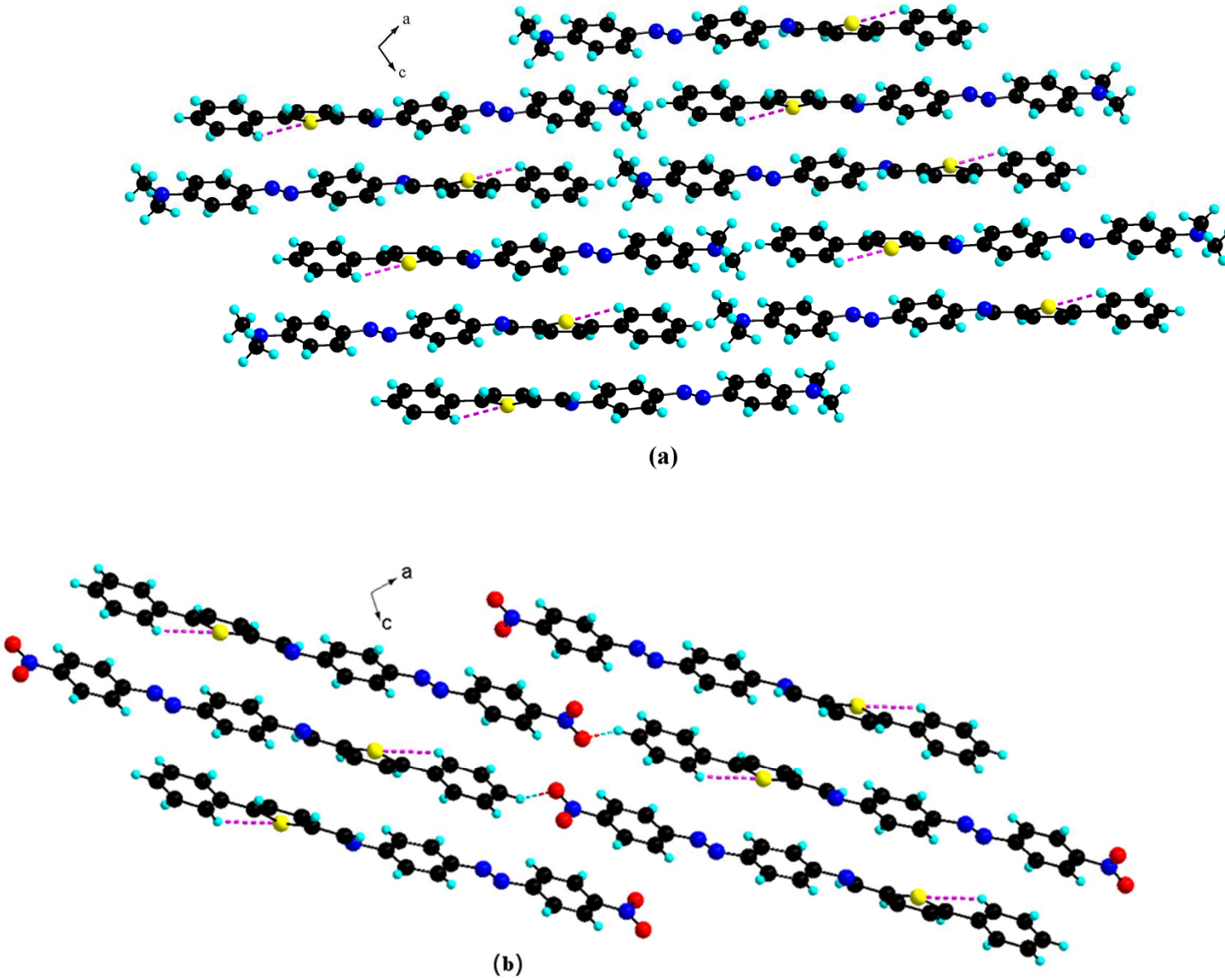

Figure 2: (a) *Supramolecular sheets in* ***A:*** C–H···S *(pink dashed lines),* ***(b)****Supramolecular sheets in* ***B:*** *C– H···O (red-cyan dashed lines).*

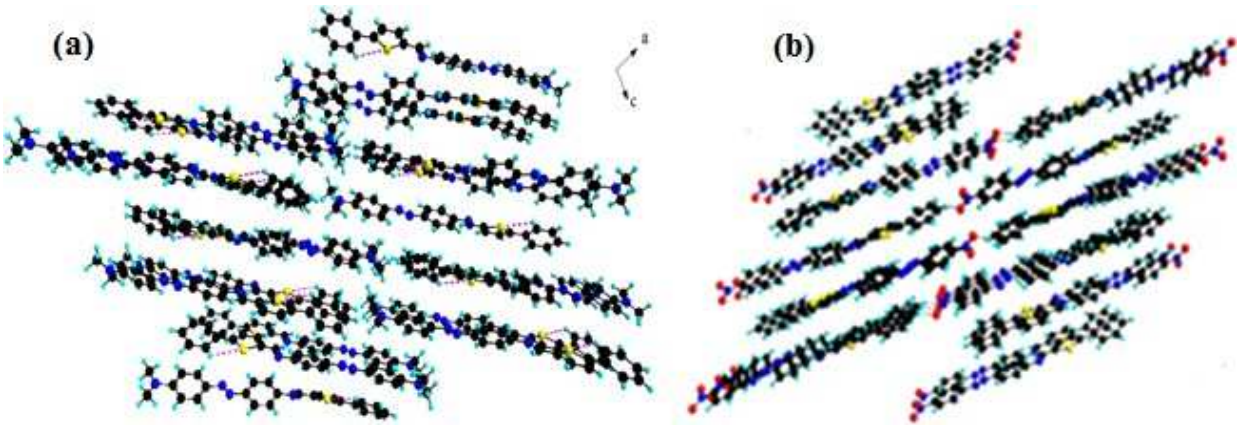

Figure 3*: Projection of the atomic arrangement of* ***A*** *(a) and* ***B*** *(b).*

In both crystal structures, π–π interactions coexist with hydrogen bonding and participate to the final stability of the molecular assemblies. As shown in **Figure (4a)**, the molecules stack in parallel infinite columns with an off-set head to tail arrangement due to π–π interactions involving, two by two, the aromatic rings of the azobenzene and the phenyl ring connecting to the thiophene fragment, from adjacent molecules (centroid···centroid: 3.6 Å and 4.7 Å) in **A**. Within compound **B**, the same behavior is observed (**Figure (4b)).**

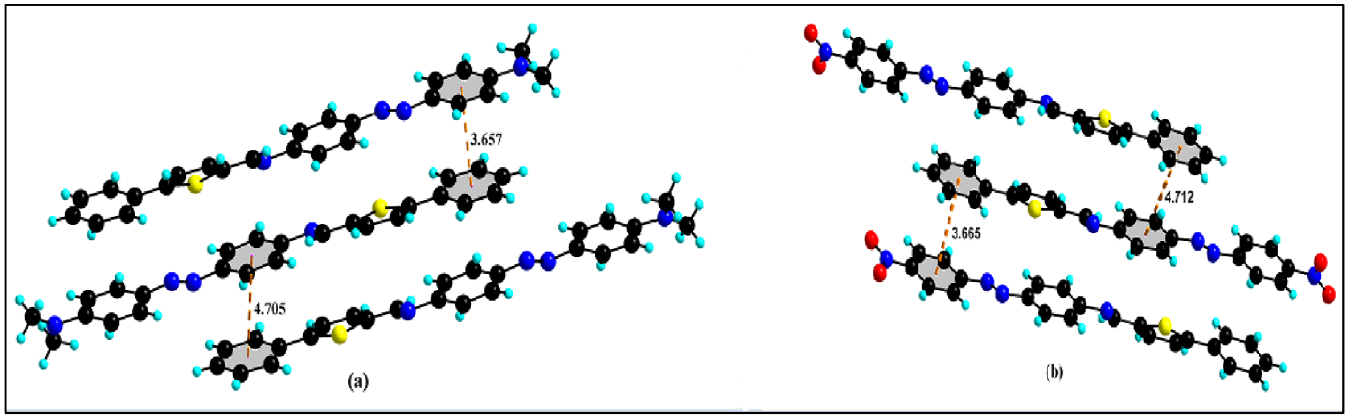

Figure 4*: Perspective of the supramolecular chain generated by offset π–π stacking between the aromatics rings (high lighted in gray) in* ***A****(a) and* ***B****(b) (centroid···centroid 3.65 and 4.7 Å).*

In the same way, the Schiff base **A** exhibits low C–H···π interactions between one atom of the amino atoms of the methyl group and the phenyl group of the neighboring molecule (see **Table 3**), as well as C–H···π between two phenylmethylamine hydrogen atoms and the same phenyl ring. The same behavior in the molecule **B**, there are a weak C–H···π interactions between two hydrogen atoms of the 4-nitrophenyl group and the phenyl ring of the neighboring molecule (see **Table 3**).

Table 1: *Crystal data and structure parameters for compounds* ***A*** *and* ***B***

Compound	**A**	**B**
CCDC No	1900208	1900209
Empirical formula	$C_{25}H_{22}N_4S$	$C_{23}H_{16}N_4O_2S$
Fw	410.52	412.46
T (K)	293	298
Crystsyst	Monoclinic	Monoclinic
Space group	P 2_1/c	P 2_1/c
a (Å)	19.844 (2)	19.904 (1)
b (Å)	5.952 (6)	5.947 (3)
c (Å)	16.577 (2)	16.569 (9)
β (deg)	101.439 (1)	101.621 (5)
V (Å^3)	1919.2 (4)	1921.25 (2)
Z	4	4
F (000)	864	865
Crystal color	Red	Red
Calc. density (g/cm^3)	1.42075	1.42589
Θ range (deg)	4.6-44.5°	2.3-72.6°
Reflns collected	3700	9018
Indep-reflns	1494	3716
Observed reflections	1144	3309
Restrains / parameters	0/272	0/272
Absorption correction type	multi-scan	multi-scan
GOF on F^2	1.08	1.09
R_{int}	0.053	0.033
final *R* indices [$I > 2\sigma(I)$]	R_1= 0.072	R_1= 0.05
	wR_2= 0.183	wR_2= 0.131
R indices (all data)	R_1=0.08	R_1= 0.054
	wR_2= 0.196	wR_2= 0.139

Table 2**: Selected bond lengths (Å) and angles (°) in **A** and **B

A		**B**	
Bond length (Å)			
C12-N1	1.416(5)	C12-N1	1.412(2)
N1-C11	1.290(6)	N1-C11	1.284(2)
C11-C10	1.436(6)	C11-C10	1.437(2)
C10-C9	1.376(6)	C10-C9	1.369(2)
C10-S1	1.724(4)	C10-S1	1.726(2)
S1-C7	1.732(4)	S1-C7	1.737(2)
C9-C8	1.405(6)	C9-C8	1.406(2)
C8-C7	1.383(6)	C8-C7	1.370(3)
C7-C6	1.459(6)	C7-C6	1.468(2)
C6-C5	1.431(6)	C6-C5	1.396(3)
C5-C4	1.383(6)	C5-C4	1.389(3)
C4-C3	1.382(7)	C4-C3	1.382(3)
C3-C2	1.396(8)	C3-C2	1.389(3)
C2-C1	1.375(6)	C2-C1	1.386(3)
C1-C6	1.388(6)	C1-C6	1.399(3)
Angle values (°)			
C12-N1-C11	117.360 (4)	C12-N1-C11	117.799(2)
N1-C11-C10	122.599(4)	N1-C11-C10	123.477(2)
C11-C10-S1	123.809(3)	C11-C10-S1	122.876(1)
C10-S1-C7	92.616(2)	C10-S1-C7	91.993(9)
C10-C9-C8	113.542(4)	C10-C9-C8	113.009(2)
C8-C7-S1	110.182(3)	C8-C7-S1	110.306(1)

Table 3: C–H···Pi interactions *(Å)*

*Cg'' is the centroid of the C1–C6 ring (**A**) and Cg' is the centroid of the C1–C6 ring (**B**)*

A				
D–H···*A*	*D*–H	H···*A*	*D*···*A*	*D*–H···*A*
C19–H19···Cg''	0.930	3.705	3.5119(3)	71
C20–H20···Cg''	0.930	3.985	3.6760(4)	64
C24–H24A···Cg''	0.960	4.659	5.0618(6)	109
B				
C19–H19···Cg'	0.930	3.748	3.5271(1)	70
C20–H20···Cg'	0.930	3.959	3.6723(1)	66

Infrared spectra

To get more information about the crystalline structure, we have made a vibration study using infrared spectroscopy. The infrared spectra, at room temperature, of two studied compounds are depicted in **Figure 5**. The spectrum of **A** and **B** display strong bands at 1608 cm $^{-1}$ and 1580 cm^{-1} respectively, attributed to the imine group (C=N). The peaks observed in the gamut of 1200-1500 cm^{-1}, for both compound, is assigned to the ν(N=N) stretching vibration of the azobenzene moiety. The IR spectrum of **A** close to 3000 cm^{-1} exhibit one peak at 2900 cm^{-1} which corresponds to CH_3 asymmetric stretching vibrations (ν_{as} (CH_3)). On the other side, in the spectrum of compound **B** this peak is absent. The (C–S) stretching vibrations of **A** and **B** are observed in 750 cm^{-1} and the bands at 550 cm^{-1} and 558 cm^{-1} respectively can be assigned to (C–C) deformation. The results of the preliminary analysis, by IR spectroscopy, of both compounds are in agreement with those obtained for the same types of compounds [25-26].

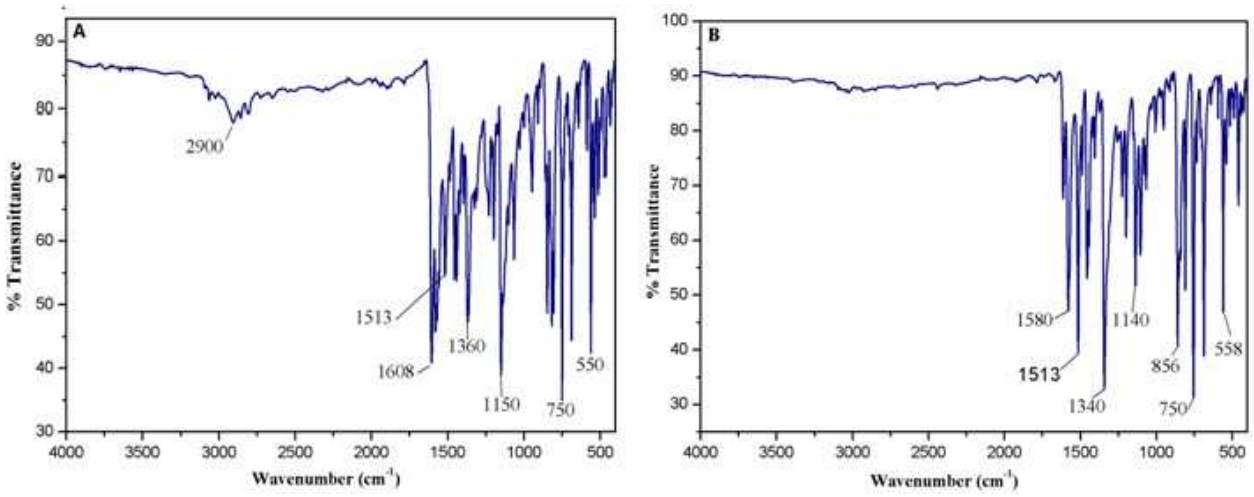

Figure5*: Infrared spectra of* ***A*** *and* ***B*** *at room temperature in the (4000-400) cm^{-1} range.*

Thermal analysis

Thermogravimetric analysis (TGA) for **A** and **B** (**Figure 6)** shows that the both compounds begin to decompose at 315 °C. In addition, no weight losses were observed between 30 and 315°C.

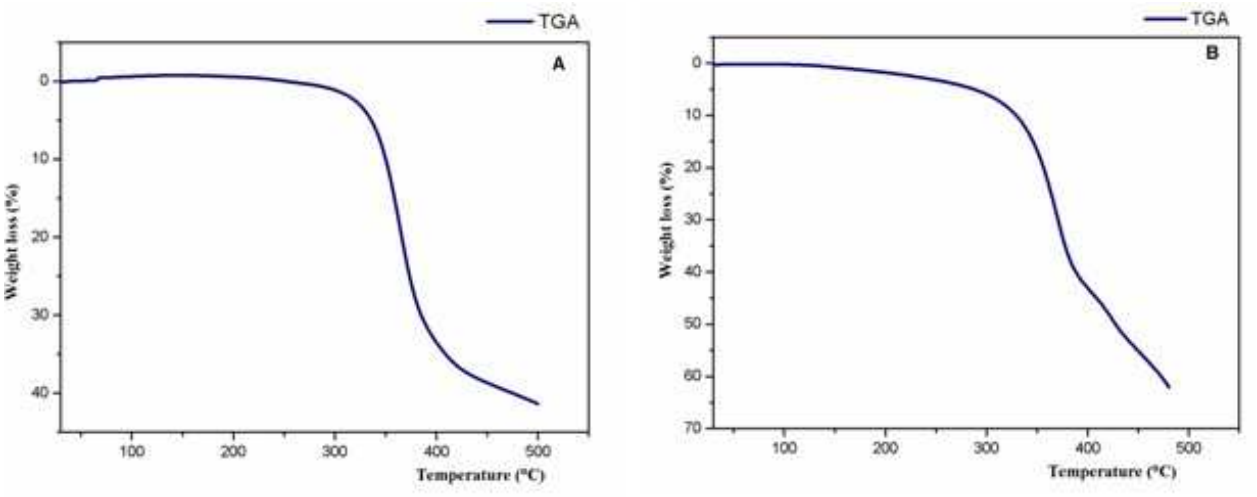

Figure 6: *TGA Curve of ligand **A** and ligand **B***

Study of intermolecular interactions via Hirshfeld surface analysis

In order to summarize the intermolecular interactions found in the studied compounds based on phenylthiophene, an analysis of the Hirshfeld surfaces of the organic systems was performed. This method is constructed based on the electron distribution calculated as the sum of spherical atom electron densities [27-28]. The breakdown of the two-dimensional fingerprint plots was used for identification of the regions of particular importance to intermolecular interactions by color coding having short or long contacts [29].

The Hirshfeld surfaces of both **A** and **B** Schiff bases are displayed respectively in **Figure 7** and **Figure 8**, showing the surface that has been mapped over d_{norm}. The Hirshfeld surface surrounding the asymmetric unit is constructed based on the electron distribution calculated as the sum of spherical atom electron densities.

For each point on that iso-surface, two distances appeared: the first one corresponds to d_e representing the distance from the point to the nearest nucleus external to the surface and the second one corresponds to d_i representing the distance to the nearest nucleus internal to the surface. The normalized contact distance (d_{norm}) based on both d_e and d_i and the van der Waals (vdw) radius of the atom is obtained from equation (1):

$$\mathbf{d_{norm} = \{(d_i - r_i^{vdw})/r_i^{vdw}\} + \{(d_e - r_e^{vdw})/r_e^{vdw}\},} \quad \mathbf{(1)}$$

Whose $\mathbf{r_i^{vdw}}$ and $\mathbf{r_e^{vdw}}$ being the van der Waals radii of the respective atoms, which are internal and external to the molecular surface.

Graphical plots of the molecular Hirshfeld surface mapped with d_{norm} use the blue–white–red color scheme, with blue revealing the longer contact distances than the sum of van der Waals radii with

positive values of d_{norm}, white indicating the contacts around the vdw separation, they indicate H···H type interactions. The red areas, depict the interatomic distances which are shorter than the sum of Van der Waals radii with negative values of d_{norm} [30].

The association between d_i and d_e in the form of a two-dimensional fingerprint plot supply a brief summary of intermolecular contacts in the compounds **A** and **B** (**Figure 9** and **Figure 10**). These analyses reveal the presence of different types of intermolecular interactions.

For the ligand **A**, the highest contribution occurs due to H···H interaction (51.4%), which are responsible for the appearance of deep white spots in the d_{norm} scheme. This proves that vdw forces exert an important influence on the stabilization of the crystal lattice packing. The second largest percentage can be attributed to the C···H /H···C (12.1%/9.3%) and C···C (9.7%).Also , other interactions contribute less to the Hirshfeld surfaces: N···H/H···N (4.9%/3.1%), S···H/H···S (3.4%/1.8%), S···C/C···S (0.4%/0.4%), S···N/N···S (0.3%/0.2%) and C···N/N···C (1.5%/1.5%), these values were calculated using Crystal Explorer program [28].

For the ligand **B**, it may also be noted that the major contribution is from H…H (34.8%). Nevertheless, they are evident, because the majority of the surface of this molecular crystal is covered by H atoms. The contribution of N···H/H···N, N···O/O···N, N···C/C···N, C···O/O···C, S···C/C···S and S···N/N···S contacts to the total Hirshfeld surface is relatively small; (5.1%/3.6%), (0.3%/0.2%), (1.7%/1.8%), (0.6%/0.5%), (0.4%/0.4%), (0.3%/0.3%), respectively. We can also report the presence of C···H/H···C close contacts, which appear in the 2D fingerprint plot comprising 19.8% of the total Hirshfeld surface of the organic molecules. Analysis of Hirshfeld surface shows the interactions between C···C and O···O with the percentages 9.9% and 0.5%, respectively of the Hirshfeld surface. Again, very low percentages of O···H/H···O (7.9%/6.6%) and S···H/H···S (3.5%/1.8%), respectively interactions are recorded in the molecule.

The presence of the adjacent red and blue triangles on the shape index surface of the two compounds **A** and **B** (surrounded by a black circle in **Figure 11**) demonstrates the presence of π–π and C-H··π stacking interactions. This result has been confirmed by X-ray crystal structural analysis.

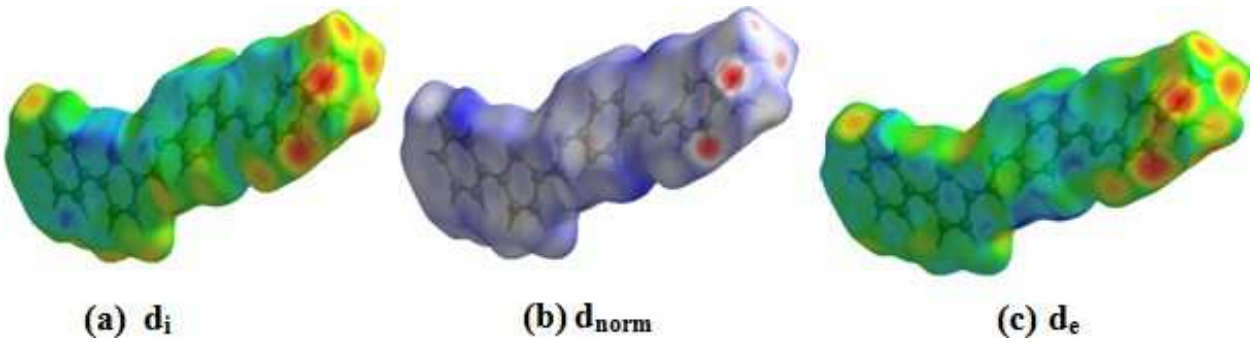

***Figure 7**: Hirshfeld surfaces analysis mapped with d_i, d_{norm} and d_e of (**A**).*

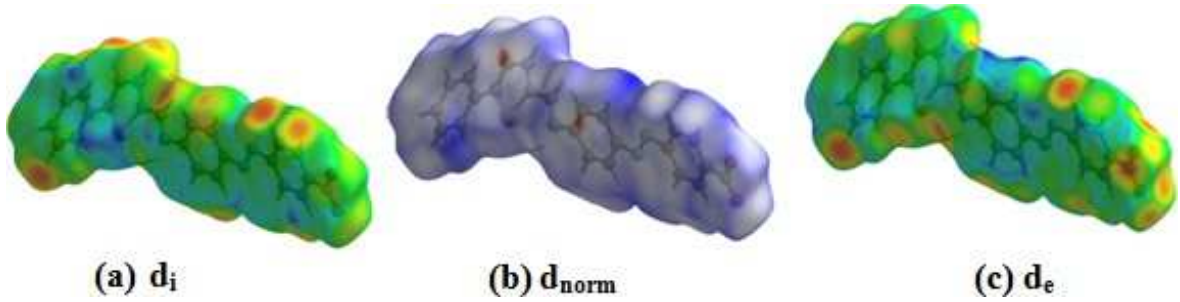

***Figure 8**: Hirshfeld surfaces analysis mapped with d_i, d_{norm} and de of (**B**).*

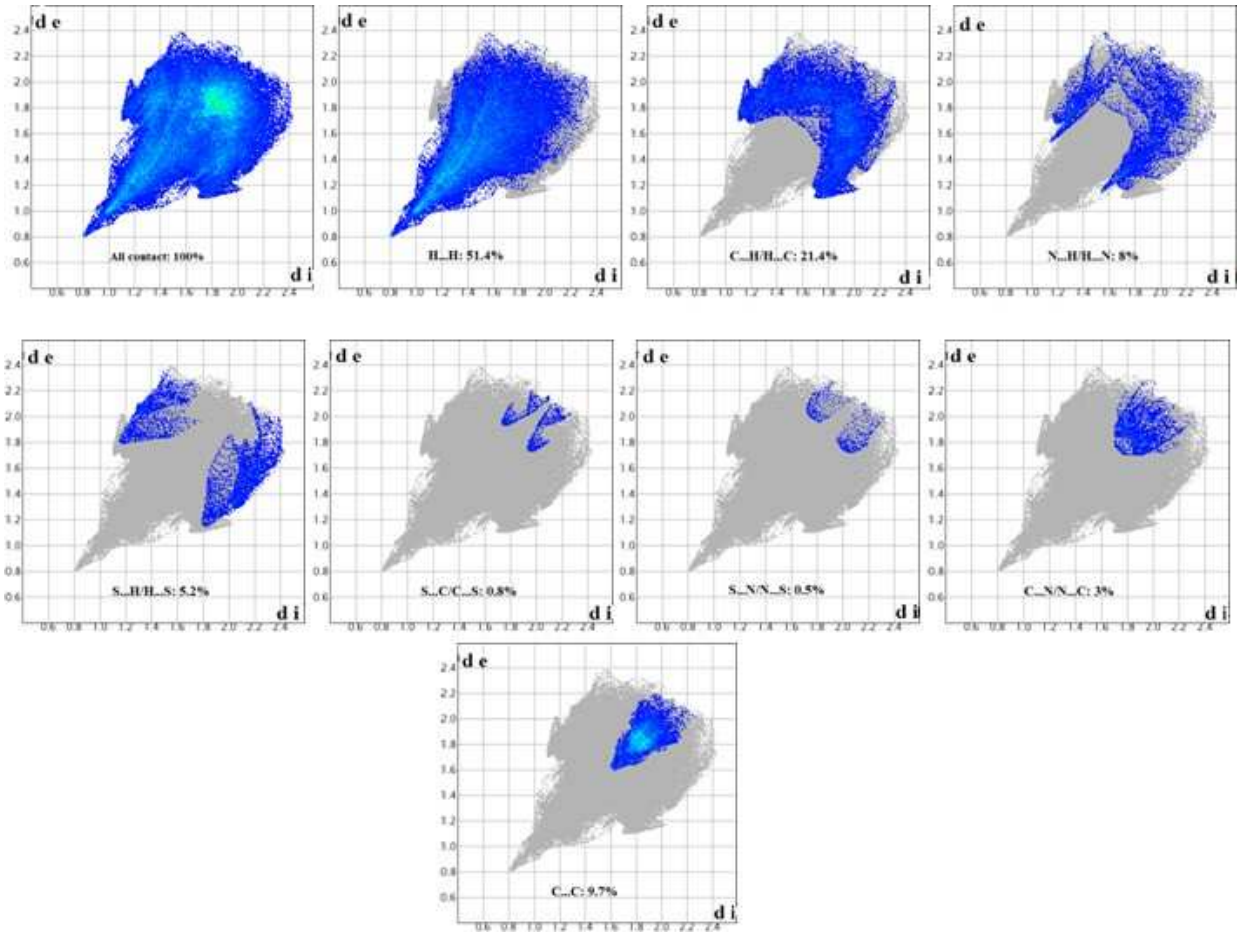

***Figure 9**: Fingerprint analysis of compound **A**.*

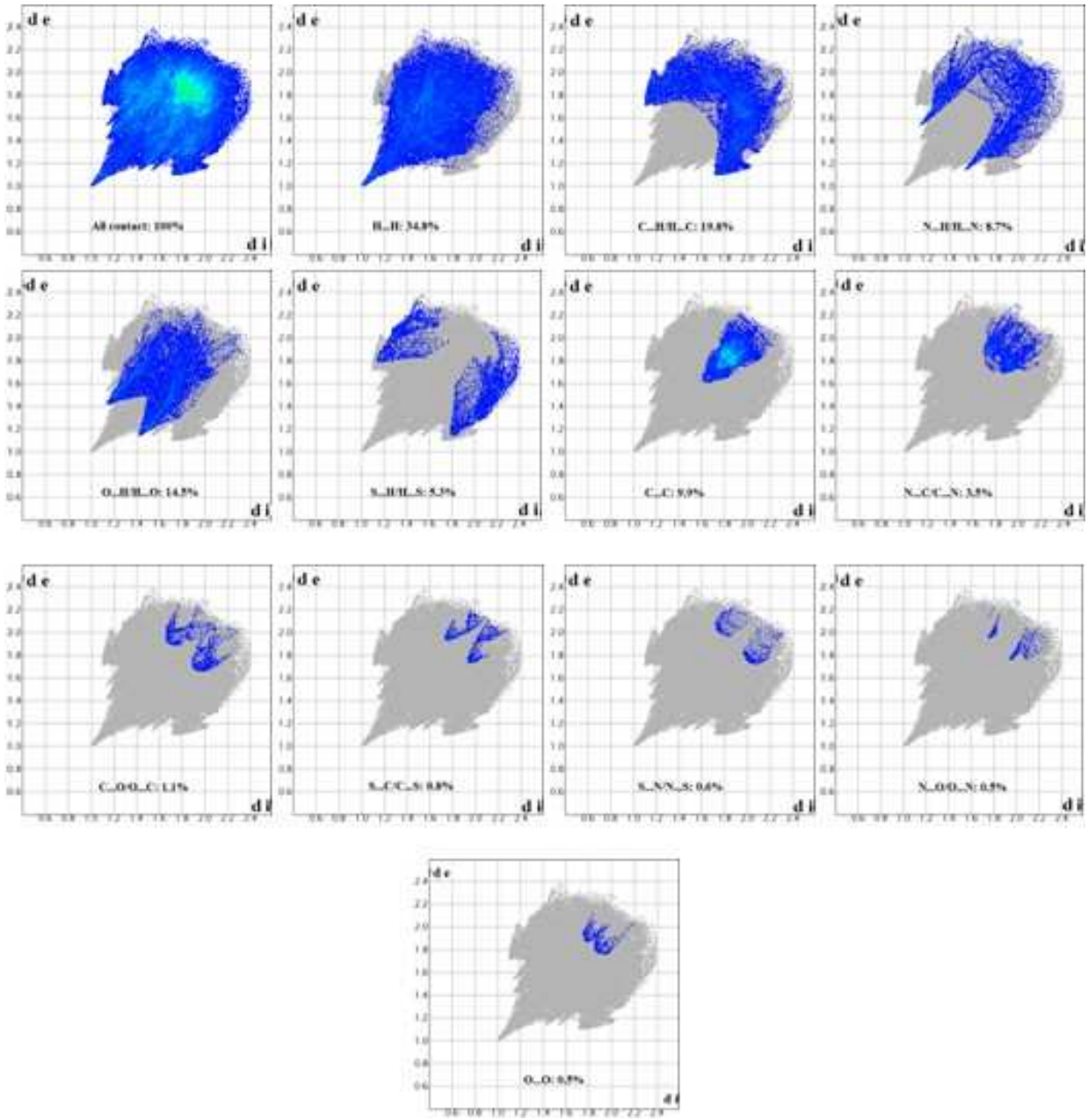

Figure 10**: Fingerprint analysis of compound **B.

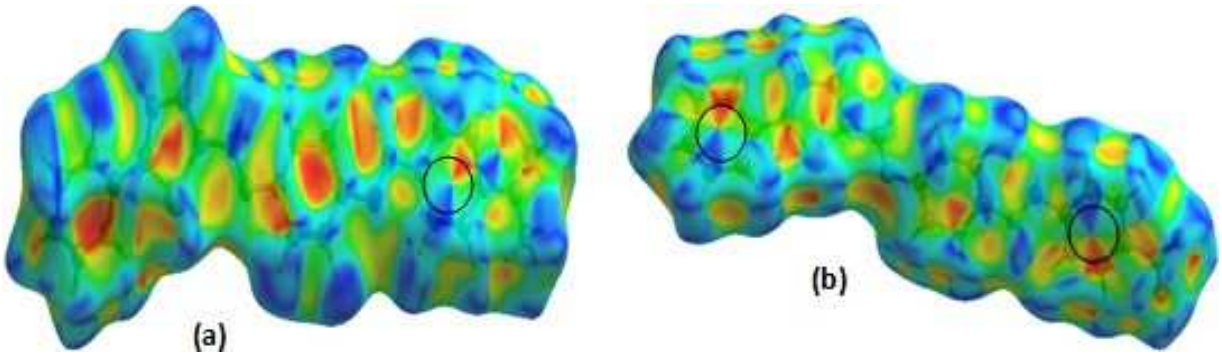

***Figure 11**: Hirshfeld surfaces in the asymmetric unit of compound **A** (a) and **B** (b), showing views of shape index.*

UV-Vis absorption studies

The UV-vis spectrum of a material provides important structural information and is a good way to examine the properties of semiconductors, as it involves the promotion of an electron from σ and π orbits of the ground state to the large energy state [31]. It gives also information about the optical band gap of the material. The energy of the forbidden band of insulators is higher than (4 eV) but less than (3 eV) for semiconductors [32]. In this case of study, **Figure 12** shows the UV-visible absorption spectra of compounds **A** and **B** that were recorded in dichloromethane solution (~ C =5×10^{-5} M) at room temperature between 250-800 nm. These spectra exhibit strong absorption bands in the visible region at around 449 nm (ε = 7326 $L.mol^{-1}.cm^{-1}$) and at around 408 nm (ε = 5205 $L.mol^{-1}.cm^{-1}$) for **A** and **B**, respectively which are assigned to the π–π* and n–π* transitions. These absorption bands in the visible region are characteristic of intramolecular charge transfer between the azobenzene fragment and phenylthiophene unit. The band for **A** indicates a stronger intramolecular charge transfer compared to **B** due to the dimethylamino donor group [33,34]. Indeed, the determination of gap energy requires the relationship of tauc's for direct and indirect optical band gap [35].

$$(\alpha h\nu)^n = k\,(h\nu - E_g)$$

Where, α is the absorption coefficient, E_g is the optical band gap, k is energy independent constant and n is a constant whish determine the type of transition (for direct band gap n=1/2 and n=2 for indirect band gap). The absorption coefficient (α) is calculated by the following relationship:

$$\alpha = 2.303A/d$$

Whose d(m) and A represent the thickness and the absorbance respectively. The measured optical band gap energies of **A** and **B** are shown in **Figure 13**. The values of the optical band gap are obtained by extrapolating the linear part of the curve between $(\alpha h\nu)^n$ (n=1/2 or n=2) and hν when α equal to zero. The permitted direct and indirect optical band gaps of the ligands **A** and **B** are 2.13, 2.17 eV for direct optical band gap and 2.36, 2.60 eV for indirect optical band gap, respectively. These results are confirmed by the literature [1, 36] and indicate that these compounds are semiconductors.

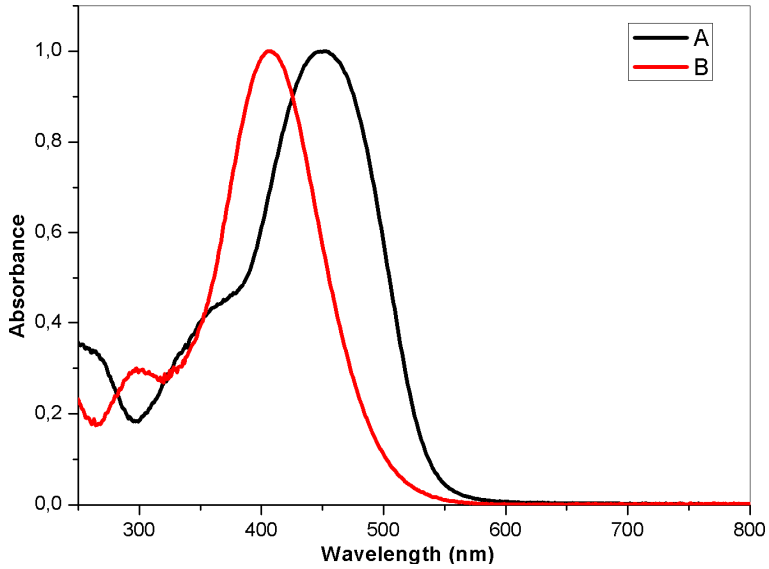

Figure 12: *UV-visible absorption spectra of* ***A*** *and* ***B*** *(C = 5×10^{-5} M) in dichloromethane at room temperature.*

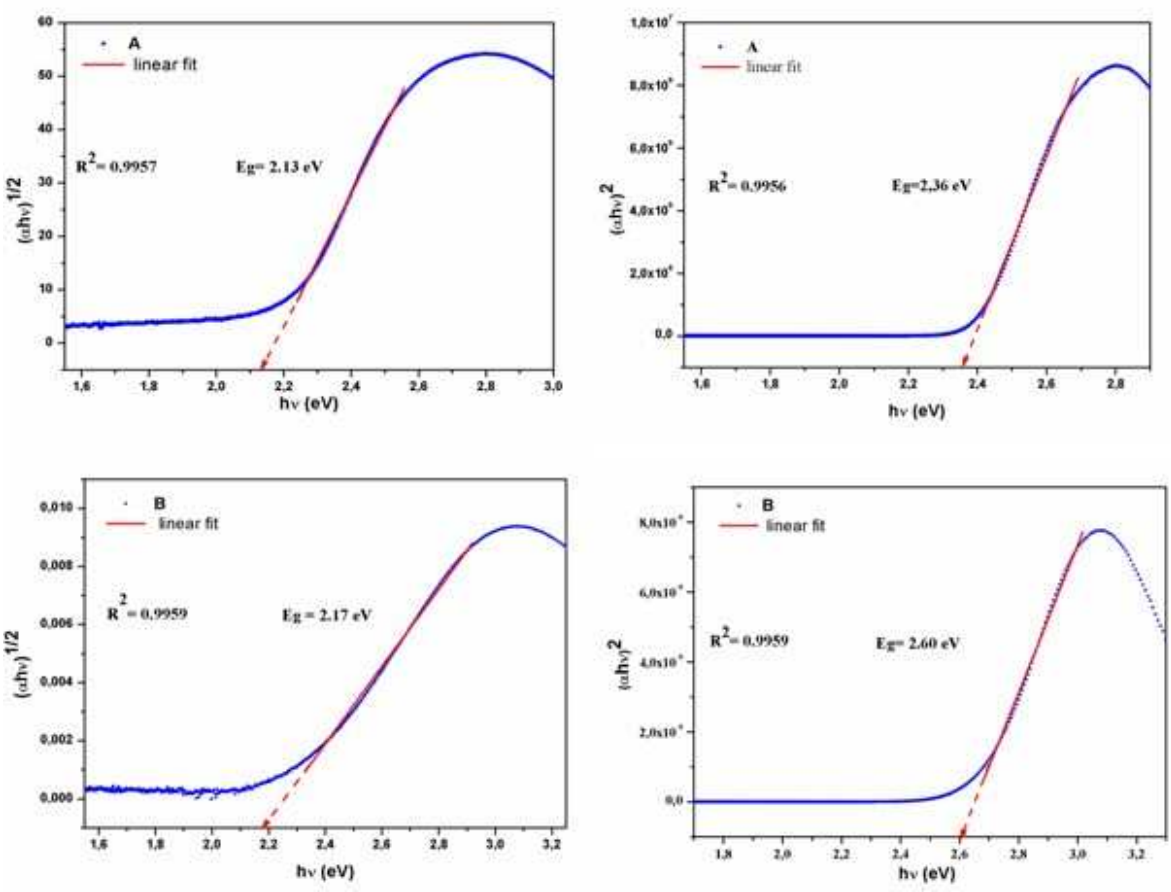

Figure 13: *Tauc plots for compounds* ***A*** *and* ***B****.*

4. Conclusion

In this work, we have prepared two multifunctional compounds based on azobenzene as photoactive unit and the phenylthiophene group. Suitable single crystals for X-ray analysis have been grown for **A** and **B** by slow diffusion of diethyl ether in dichloromethane solution. The result of single X-ray diffraction demonstrates that the two Schiff bases crystallize in the monoclinic system space group $P2_1/c$. The molecules stack in parallel infinite columns with an off-set head to tail arrangement. Hirshfeld surface analysis shows different types of intermolecular interactions including hydrogen bonding, π–π stacking and C–H···Cg interactions. This study has highlighted the importance of H···H and C···H contacts in the structure, which constitute, one-half and one-quarter of the interactions present in **A** and one-third and one-quarter of the interactions present in **B**. These two compounds were characterized by UV-Vis spectroscopy and the optical band gap was calculated by the tauc's model. The values of the optical band gap energy for **A** and **B** are 2.13, 2.17 eV for direct optical band gap and 2.36, 2.60 eV for indirect optical band gap, respectively, which confirms that this compounds present a semiconducting behavior. The results reported herein suggest that these two Schiff bases can be used as active materials for organic electronics (transisitors, OLEDs, solar cells…).

References

[1] J-L. Bredas, D. Beljonne, V. Coropceanu, J. Cornil, Charge-Transfer and Energy-Transfer Processes in π-Conjugated Oligomers and Polymers: A Molecular Picture, Chem. Rev, 104 (2004) 11, 4971-5004, https://doi.org/10.1021/cr040084k.

[2] K.Staub, G.A Levina, S. Barlow, T. C. Kowalczyk, H. S. Lackritz, M. Barzoukas, A. Fort, S. R. Marder, Synthesis and stability studies of conformationally locked 4-(diarylamino)aryl- and 4-(dialkylamino)phenyl-substituted second-order nonlinear optical polyene chromophores, Mat. Chem, 13 (2003) 825-833, https://doi.org/10.1039/B208024A.

[3] H.E.A. Huitema, G.H. Gelinck, J.B.P.H. van der Putten, K.E. Kuijk, C.M. Hart, E. Cantatore, D.M. de Leeuw, Active-Matrix Displays Driven by Solution-Processed Polymeric Transistors, Advan. Mat, 14 (2002) 1201-1204, https://doi.org/10.1002/1521-4095(20020903)14:17<1201::AID-ADMA1201>3.0.CO;2-5.

[4] D.T. McQuade, A. H. Hegedus, T. M. Swager, Signal Amplification of a "Turn-On" Sensor: Harvesting the Light Captured by a Conjugated Polymer, J. Am. Chem. Soc., 122 (2000) 12389-12390, https://doi.org/10.1021/ja003255l.

[5] D. T. McQuade, A. E. Pullen, T. M. Swager, Conjugated Polymer-Based Chemical Sensors, J. Am. Chem. Soc., 100 (2000) 2537-2574, https://doi.org/10.1021/cr9801014.

[6] E. Merino, M. Ribagorda, Control over molecular motion using the cis–trans photoisomerization of the azo group, Org. Chem, 8 (2012) 1071–1090, https://doi:10.3762/bjoc.8.119.

[7] A. A. Beharry, G. A. Woolley, Azobenzene photoswitches for biomolecules, Chem Society Rev, 40 (2011) 4422–4437, https://doi.org/10.1039/C1CS15023E.

[8] J. García-Amorós, D. Velasco, Recent advances towards azobenzene-based light-driven real-time information-transmitting materials, Org Chem, 8 (2012) 1003–1017, https://doi:10.3762/bjoc.8.113.

[9] T. Muraoka, K. Kinbara, Y. Kobayashi, T. Aida, Light-Driven Open–Close Motion of Chiral Molecular Scissors, J. Am. Chem. Soc., 125 (2003) 5612-5613, https://doi.org/10.1021/ja034994f.

[10] N.Liaros, S. Couris, L. Maggini, F. De Leo, F. Cattaruzza, C. Aurisicchio, D. Bonifazi, NLO response of photoswitchable azobenzene-based materials, Phys. Chem. Phys. Chem., 14 (2013) 13, 2961-2972, 10.1002/cphc.201300420.

[11] H. El Ouazzani, K. Iliopoulos, M. Pranaitis,O. Krupka, V. Smokal, A. Kolendo, B. Sahraoui, Second- and Third-Order Nonlinearities of Novel Push–Pull Azobenzene Polymers, Phys. Chem. B, 115 (2011) 1944-1949, https://doi.org/10.1021/jp109936t.

[12] A. Natansohn, P. Rochon, Photoinduced Motions in Azo-Containing Polymers, Chem. Rev, 102 (2002) 4139-4175, https://doi.org/10.1021/cr970155y.

[13] A.G. Cheelham, M.G. Hutchings, T.D.W. Claridge, H.L. Anderson, Enzymatic Synthesis and Photoswitchable Enzymatic Cleavage of a Peptide-Linked Rotaxane, Angew. Chem. Int. Ed., 45 (2006) 1596-1599, https://doi.org/10.1002/anie.200504064.

[14] H. Nishihara, Combination of redox- and photochemistry of azo-conjugated metal complexes, Coord. Chem. Rev. 249 (2005) 1468-1475, https://doi.org/10.1016/j.ccr.2004.11.009.

[15] Y.H. Zhou, P. Peng, L. Han, W.J. Tian, Novel donor–acceptor molecules as donors for bulk heterojunction solar cells, Synth. Met., 157 (2007) 502-507, https://doi.org/10.1016/j.synthmet.2007.05.012.
[16] A. Kleemann, J. Engel, B. Kutscher, D. Reichert, Pharmaceutical Substances: Syntheses, Patents Applications, Org. Process Res. Dev., 6 (2002) 739-740, https://doi.org/10.1021/op0200423.
[17] M.C. Silva Lourenco, F. Rodrigues Vicente, M.G. de Oliveira Henriques, A.L. PeixotoCandea, R.S. Borges Goncalves, T.C.Nogueira, M. de Lima Ferreira, M.V. Nora de Souza, Synthesis and biological evaluation of N-(aryl)-2-thiophen-2-ylacetamides series as a new class of antitubercular agents, Bioorg. Med. Chem. Lett, 17 (2007) 6895-6898, https://doi.org/10.1016/j.bmcl.2007.09.096.
[18] A.M. Khalil, M.A. Berghot, M.A. Gouda, Synthesis and antibacterial activity of some new thiazole and thiophene derivatives, Bioorg. Med. Chem. Lett., 44 (2009) 4434-4440, 10.1016/j.ejmech.2009.06.002.
[19] J. Roncali, Conjugated poly(thiophenes): synthesis, functionalization, and applications, Chem Rev, 92 (1992) 711-738, https://doi.org/10.1021/cr00012a009.
[20] H. S. Nalwa, Organic Materials for Third-Order Nonlinear Optics, Adv Mat, 5 (1993) 341-358, https://doi.org/10.1002/adma.19930050504.

[21] L. J. Farrugia, WinGX suite for small-molecule single-crystal crystallography, J. Appl. Cryst., 32 (1999) 837-838, https://doi.org/10.1107/S0021889899006020.

[22] G. M. Sheldrick, SHELXS-97: Programs of Crystal solution, University of Gottingen, Germany (1998).
[23] Brandenburg, K. (2006). DIAMOND. Crystal Impact GbR, Bonn, Germany.
[24] S.K. Wolff, D.J. Grimwood, J.J. McKinnon, M.J. Turner, D. Jayatilaka and M.A. Spackman, Crystal Explorer 3.1,University of Western Australia (2012).
[25] A.S. Abu-Khadra1, R. S. Farag, A. El-Dine Mokhtar Abdel-Hady, Synthesis, Characterization and Antimicrobial Activity of Schiff Base (E)-N-(4-(2-Hydroxybenzylideneamino) Phenylsulfonyl) Acetamide Metal Complexes, Am. J. Anal. Chem, 7 (2016) 233-245, 10.4236/ajac.2016.73020.
[26] R.K. Agarwal, B. Prakash, V. Kumar and A. Aslam Khan, J. Iran. Chem. Soc, 4 (2007) 114-125, https://doi.org/10.1007/BF03245809.
[27] M.A. Spackman, P.G. Byrom, A novel definition of a molecule in a crystal, Chem Phys. Lett., 267 (1997) 215–220, https://doi.org/10.1016/S0009-2614(97)00100-0.
[28] J.J. McKinnon, A.S. Mitchell, M.A. Spackman, Hirshfeld Surfaces: A New Tool for Visualising and Exploring Molecular Crystals, Chem. Eur. J., 4 (1998) 2136- 2141, https://doi.org/10.1002/(SICI)1521-3765(19981102)4:11<2136::AID-CHEM2136>3.0.CO;2-G.
[29] A.L. Rohl, M. Moret, W. Kaminsky, K. Claborn, J.J. Mckinnon, B. Kahr, Hirshfeld Surfaces Identify Inadequacies in Computations of Intermolecular Interactions in Crystals: Pentamorphic 1,8-Dihydroxyanthraquinone, Cryst. Growth Des., 8 (2008) 4517-4525, https://doi.org/10.1021/cg8005212.
[30] J. J. Koenderink, A. J. van Doorn, Surface shape and curvature scales, Image Vi.s Comput, 10 (1992) 557-564, https://doi.org/10.1016/0262-8856(92)90076-F.

[31] K. Mangaiyarkarasi, A.T. Ravichandran, K. Anitha, A. Manivel, Synthesis, growth and characterization of L-Phenylalaninium methanesulfonate nonlinear optical single crystal, J. Mol. Struc., 1155 (2018) 758-764, https://doi.org/10.1016/j.molstruc.2017.11.065.
[32] G. A. Evingür, Ö. Pekcan, Optical energy band gap of PAAm-GO composites, Comp. struc, 183 (2018) 212-215, https://doi.org/10.1016/j.compstruct.2017.02.058.
[33] I.Guezguez, A. Ayadi, K. Ordon, K. Iliopoulos, D. G. Branzea, A. Migalska-Zalas, M. Makowska-Janusik, A. El-Ghayoury, B. Sahraoui, Zinc Induced a Dramatic Enhancement of the Nonlinear Optical Properties of an Azo-Based Iminopyridine Ligand, J. Phys. Chem. C, 118 (2014) 7545−7553, https://doi.org/10.1021/jp412204f.
[34] A. Ayadi, D. G. Branzea, M.A. Benmensour, A. Boucekkine, N. Zouari, A. El-Ghayoury, Azo- based iminopyridine ligands: synthesis, optical properties, theoretical calculations and complexation studies, Tetrahedron, 71 (2015) 7911-7919, https://doi.org/10.1016/j.tet.2015.08.006.

[35] P. Harvey, C. Reber, Distortions in square-planar palladium(II) halides: A nonempirical molecular orbital model study, Can. J. Chem, 77 (1999) 16-23, https://search.proquest.com/docview/218641977?accountid=17229.

[36] Y. Q. Yan, L. Xu, J. Zhang, Energy gaps and half-metallicity in β-graphyne nanoribbons, Phys. Lett. A, 383 (2019) 1498-1501, https://doi.org/10.1016/j.physleta.2019.01.052.